Version of Record: https://www.sciencedirect.com/science/article/pii/S0967064518300043
Manuscript_7e27b8969094caaa29930d7362f79c58

The encoding of wind forcing into the Pacific-Arctic pressure head, Chukchi Sea ice retreat and late-summer Barrow Canyon water masses

Stephen Okkonen
University of Alaska Fairbanks
Fairbanks, Alaska 99775
srokkonen@alaska.edu

Carin Ashjian
Woods Hole Oceanographic Institution
Woods Hole, Massachusetts 02543
cashjian@whoi.edu

Robert G. Campbell
University of Rhode Island
Narragansett, Rhode Island 02882
rgcampbell@uri.edu

Philip Alatalo
Woods Hole Oceanographic Institution
Woods Hole, Massachusetts 02543
palatalo@whoi.edu

Corresponding author:
Stephen Okkonen
Institute of Marine Science
University of Alaska Fairbanks
Fairbanks, Alaska 99775
srokkonen@alaska.edu
907-283-3234

Keywords: Chukchi Sea, Barrow Canyon, Hydrography, Sea Ice

Abstract

Barrow Canyon, which incises the northeast corner of the Chukchi Sea shelf, is a major conduit through which Pacific-origin waters carrying nutrients, biota, freshwater, and heat enter the Arctic Ocean. As such, Barrow Canyon was adopted as a long-term monitoring site for the Distributed Biological Observatory (DBO) in 2010. However, annual hydrographic surveys across Barrow Canyon, conducted during late August 2005-2015 along a location near what is the Barrow Canyon DBO survey line and in support of other research programs, extend and complement the DBO hydrographic record. These complementary hydrographic surveys show that volumes of Pacific-origin and melt water masses in Barrow Canyon are significantly-correlated with daily sea ice areas in the eastern Chukchi Sea for most of the May-August ice retreat season. Year-to-year differences in the timing and pattern of sea ice retreat across the Chukchi Sea are also shown to be well-correlated with changes in seasonally-averaged regional winds particularly as defined by the strength and longitudinal location of the Beaufort Sea High pressure cell. These interdependent wind-ice retreat-water mass relationships are largely predicated on wind stress curl-driven changes to sea level in the East Siberian Sea/northwestern Chukchi Sea. Statistically-significant correlations among wind-forced sea surface heights, ice areas, and water mass volumes suggest that, during the ice retreat season, the East Siberian Sea/western Chukchi Sea region serves as the Arctic terminus for the Pacific-Arctic pressure head.

1. Introduction

Pacific-origin waters are key drivers of the western Arctic marine ecosystem (see Fig. 1a for regional geography and place names), carrying nutrients, biota, freshwater, and heat across the Bering and Chukchi Sea shelves to the Arctic basin (Danielson et al., 2017). They support high production across these shelves (Walsh et al., 1989; Springer and McRoy, 1993), contribute to the maintenance of the Arctic halocline and the freshwater balance of the Arctic Ocean (Woodgate et al., 2005), and promote the seasonal melt back of sea ice in the Chukchi Sea (Ahlnas and Garrison, 1984). Because the duration and extent of seasonal sea ice influences the modification of Pacific-origin waters as they cross these shelves (Weingartner et al., 1998; 2005; Woodgate et al., 2005) and the trophic pathways by which organic carbon migrates through the food web, the marine ecosystems of these shelves and the Arctic Ocean are likely to be particularly responsive to a changing climate (Grebmeier et al., 2010). For example, abundances of Pacific-origin zooplankton traversing the Chukchi Sea have been increasing over the last decade, potentially impacting zooplankton species composition and, ultimately, carbon transformations (e.g., Ershova et al., 2015; Matsuno et al., 2015; Wassmann et al., 2015).

In one sense, Pacific-origin waters carried northward through Bering Strait are comprised of natal water masses named for their source regions: Anadyr Water, Bering Sea Water and Alaskan Coastal Water. An alternate nomenclature that reflects seasonal modification of these water masses during their residence on the Chukchi shelf identifies the Pacific-origin waters as Winter Water (WW), Chukchi Summer Water (CSW) and Alaskan Coastal Water (ACW). These waters arrive at Barrow Canyon driven in the mean by the Pacific-Arctic pressure head (Coachman and Aagaard, 1966; Stigebrandt, 1984; Coachman and Aagard, 1988; Woodgate, 2005). Northward transport is greatest in summer when regional winds augment or only weakly oppose the pressure head-driven flow, while northward transport in winter is minimal or reversed under stronger winds from the north (Woodgate et al., 2005). Prevailing understanding of summer circulation on the Chukchi shelf indicates that these water masses tend to follow three generalized pathways during their transits across the Chukchi Sea (Spall, 2007; Brugler et al., 2014). Cold, salty WW and somewhat warmer, fresher CSW flow along two routes, with stronger flow occurring through Herald Canyon in the western Chukchi (Coachman et al., 1975) and weaker flow through the Central Channel in the central Chukchi (Weingartner et al., 2005). ACW, the warmest water mass, is preferentially carried along the Alaskan Chukchi coast by the Alaskan Coastal Current (Paquette and Bourke, 1974). Although waters following these three advective pathways converge with some regularity in the northeastern Chukchi Sea and exit the shelf through Barrow Canyon (Weingartner et al., 2005; Winsor and Chapman, 2004; Spall, 2007, Pickart et al., 2016), there remains considerable uncertainty as to how transport variability among these pathways is manifested as transport and hydrographic variability in Barrow Canyon.

While hydrographic and transport variability in Barrow Canyon have often been addressed in relation to local winds (e.g., Weingartner et al., 2005, 2013; Okkonen et al., 2009; Itoh et al., 2013; Itoh et al., 2015; Pickart et al., this issue), in this paper we show that remote wind-forcing is also important to understanding (observed) hydrographic and (inferred) transport variability in the canyon. Year-to-year (2005-2015) differences in the late-summer volumes of archetypal water masses in Barrow Canyon occur due to wind-induced changes to the Pacific-Arctic pressure head and the consequent differences in the timing and trajectory of sea ice retreat across the Chukchi Sea. Barrow Canyon is one of sites of the Distributed Biological Observatory (DBO) program (Moore and Grebmeier, 2017) that has been designed as a "change detection array" to identify biological responses to changing physical characteristics of the Pacific Arctic. Although the hydrographic data used in our analyses were acquired in support of other research programs, these data complement and extend the DBO hydrographic record in Barrow Canyon.

2. Data

2.1 Geographical Setting

Our study area within the Pacific Arctic is bounded by the 55°N and 80°N parallels and the 160°E and 120°W meridians (Fig. 1a) . Within this study area, we delineate the Chukchi Sea shelf domain as being bounded by the Bering Strait (~65.8°N) in the south, the 150-m isobath in the north, the 180° meridian in the west and the 156°W meridian in the east.

2.2 Hydrography

In support of various field programs (see Acknowledgments), hydrographic surveys across Barrow Canyon in the northeast Chukchi Sea were conducted annually (2005-2015) within a few days before or after 22 August from a small (<15 m) coastal research vessel (R/V *Annika Marie* or R/V *Ukpik*) along a transect extending ~40 km northwestward from Point Barrow (Fig. 1b).

This transect lies close (~25 km northeast) to the DBO 5 line. Because of the small vessel size, these hydrographic surveys were all conducted during relatively benign wind conditions (4.7 +/- 1.1 m s^{-1}, mean +/- S.D.). As a consequence, with the exception of the 2013 survey, the flow was down-canyon on the east side and weakly up-canyon on the west side (Supplementary Figure 1). Weak up-canyon flow was observed across most of the section during the 2013 survey. Temperature and salinity measurements were acquired using both a Seabird 19plus lowered Conductivity-Temperature-Depth (CTD) recorder and a towed Acrobat profiling vehicle equipped with a Seabird 49 CTD. Details of the hydrographic sampling methodology are described in Okkonen et al. (2009).

Temperatures (T) and salinities (S) encountered in Barrow Canyon during these surveys ranged from $-1.8°C < T < 10.6°C$ and from $23.3 < S < 34.9$, respectively. For this region of T/S space, we adopt with some minor modifications the water mass classification scheme of Gong and Pickart (2015). The focal water masses for this study are sea ice meltwater and three Pacific-origin water masses. Late season meltwater (LMW), overall the freshest water mass, is characterized by temperatures $-1°C \leq T < 7°C$ and salinities $S < 30$. Pacific-origin water masses include Alaskan Coastal Water (ACW), Chukchi Summer Water (CSW) and Pacific Winter Water (WW). ACW is characterized by relatively warm waters with temperatures $T \geq 3°C$ and salinities $S \geq 30$. A small volume of water encountered near Point Barrow in 2012 with $T \geq 7°C$ and $S < 30$ was also classified as ACW. The coldest water ($T < -1°C$, $S \geq 31.5$) encountered in Barrow Canyon is WW. Our WW classification combines two winter water masses from the Gong-Pickart classification scheme (Remnant Pacific Winter Water and Newly-ventilated Pacific Winter Water) into a single water mass. CSW, arising from a transformation of WW through solar heating and vertical mixing of open water, is characterized by temperatures intermediate to ACW and WW (-1°C $\leq$ T < 3°C) and by salinities 30 $\leq$ S <33. Other water masses encountered but not included in subsequent analyses because of their small volumes were early season melt water (EMW; T < -1°C, S < 31.5) and polar halocline/Atlantic Water (PH/AW; -1°C $\leq$ T < 1°C, 33 $\leq$ S <35).

Each year's temperature and salinity data from Barrow Canyon were interpolated to a common, regularly-spaced 1-km horizontal by 1-m vertical grid (each grid cell represents a volume of 1000 m^3). Each grid cell was then assigned one of the six water masses (described above) based on the cell's T/S characteristics. The grid cell volumes associated with each water mass in each sampling year were summed over the upper 120 m of the water column, the deepest sampling depth common to the 2005-2015 hydrographic surveys, to provide comparable statistical measures related to these focal water mass volumes.

2.3 Sea ice

Daily sea ice concentrations were obtained from the ¼° gridded NOAA High-resolution Blended Analysis of Daily SST and Ice dataset (https://www.esrl.noaa.gov/psd/data/gridded/data.noaa.oisst.v2.highres.html; Reynolds et al., 2007). Chukchi Sea ice concentrations from this dataset were unusually low from 27 April - 15 May 2009 and unrealistically high from 12 August -16 August 2012 and were considered suspect. Daily ice concentration data at each ¼° grid point during these periods thus were replaced with concentrations linearly interpolated between reasonable concentrations occurring on 26 April and 16 May 2009 and on 11 Aug 2012 and 17 Aug 2012. Daily Chukchi sea ice areas were then computed as the sum of the fractional ice concentration-weighted areas of the grid cells within the Chukchi shelf domain.

2.4 Meteorology

The 2.5° gridded NCEP/NCAR Reanalysis 1 data set (https://www.esrl.noaa.gov/psd/data/gridded/data.ncep.reanalysis.html; Kalnay et al., 1996) provided daily sea level pressure (SLP) and surface U and V winds. We computed wind stresses using a standard quadratic formula with an air-water drag coefficient of 0.0013. We did not adjust the stress computations to account for ice concentrations directly or through a larger ice concentration-weighted drag coefficient (e.g. Hibler, 1980) or to account for internal ice stresses (Martin et al., 2014). Daily Ekman pumping velocities were derived from wind stress curl (WSC) calculations at each NCEP grid point within the study domain using a central difference formula in which $\Delta x = 10°$ (1110 km x cos(latitude)) and $\Delta y = 5°$ (555 km).

3. Results

3.1 Water mass volumes and Chukchi sea ice

Cross-canyon distributions of water mass volumes exhibited substantial variability over the 11-year record (Fig. 2; corresponding annual temperature and salinity fields are depicted in Supplementary Figures S2-S3). In some years (2005, 2007, 2011, 2015) the dominant surface water mass was warm ACW, whereas in other years (2006, 2008, 2009, 2013, 2014) cool, fresh LMW was the dominant surface water mass. This warm-cold dichotomy also extends below the surface within Barrow Canyon. Years in which cold WW volumes are anomalously low tend to be years in which warmer CSW and/or ACW volumes are anomalously high and vice versa (Fig. 3a-d). Corresponding records of east Chukchi sea ice areas at the approximate midpoint (1 July) and end (11 August) of the ice retreat season (defined below) are shown in Figure 3e. Covariance between ACW and LMW and among other focal water mass volumes over the 2005-2015 period occurred at statistically-significant levels (Table 1, $p < 0.05$ or better), except for ACW and CSW.

Table 1 *Correlations among water mass volumes in the upper 120 m across Barrow Canyon. Statistically-significant correlations are highlighted in italicized ($|r| > 0.521$, $p < 0.05$) and bold ($|r| > 0.685$, $p < 0.01$; 9 degrees of freedom) text.*

	ACW	**CSW**	**WW**
LMW	**-0.70**	*-0.58*	**0.69**
ACW		0.24	**-0.82**
CSW			**-0.72**

Consideration of the covariant relationships among these water masses in the context of

1) heat supplied by the northward flow of Pacific-origin water masses through Bering Strait contributing to the retreat of sea ice across the Chukchi shelf (Ahlnas and Garrison, 1984),
2) the different advective paths followed by Pacific-origin water masses across the shelf (Spall, 2007; Brugler et al., 2014) and
3) sea ice-mediated transformation of WW during its residency on the shelf (Weingartner et al., 1998; 2005; Woodgate et al., 2005)

suggests that year-to-year differences among the water mass volumes in Barrow Canyon reflect year-to-year differences in the timing and pattern of sea ice retreat across the Chukchi shelf.

We investigated the pattern and timing of sea ice retreat through iterative correlation analyses. Coefficients were sequentially calculated for correlations between the eleven-year time series of each late-August focal water mass volume and daily sea ice area from 1 April to 21 August (the median date of hydrographic sampling) in a set of 10° longitude-wide (380 km at 70°N) overlapping sections of the Chukchi shelf. The western edge of the 10° shelf section was advanced in 0.25° steps from 170°E to 166°W, resulting in 97 sections. The ice area date was advanced one day at a time and correlations between water mass volumes and daily ice area were calculated for each of the 97 sections. The strongest aggregate correlations were between water mass volumes and daily sea ice areas within the 10°-wide section of the eastern Chukchi shelf between 169°W and 159°W (Fig. 4). Daily sea ice areas in the eastern Chukchi and late-August LMW volumes (solid line) are significantly positively correlated ($r > 0.521$, $p < 0.05$ level or better) from mid-May to late August. Correlations between WW (dash-dot line) and ACW (dotted line) volumes and daily eastern Chukchi ice areas are significant from late May to mid-July and again in early August, with positive correlations ($r > 0.521$) between ice area and WW and negative correlations ($r < -0.521$) between ice area and ACW. CSW volumes (dashed line) and daily eastern Chukchi ice areas are significantly negatively correlated ($r < -0.521$) for shorter periods in late May to early June and late June to early July. The average of correlations between daily sea ice areas in the eastern Chukchi and late-August water mass volumes exceed $|r| > 0.521$ from 27 May to 11 August. We adopt these dates as start and end dates for a common period of the ice retreat season over which integrated forcing acts to define characteristic patterns and histories of sea ice retreat across the eastern Chukchi shelf and corresponding late-summer distributions of water mass volumes in Barrow Canyon.

Daily sea ice area histories from April 1 through the third week in August for each year reveal differences in the timing of seasonal sea ice retreat across the eastern Chukchi shelf between 169°W and 159°W (Fig. 5). Sea ice areas were similar in all years on 1 April, but start to diverge by late April. From 27 May to 11 August, the retreat histories defining slower/later sea ice retreats (solid lines) and faster/earlier retreats (dotted lines) are largely differentiated from one another. Greater daily sea ice extents and slower/later sea ice retreats occurred in years (2006, 2008, 2009, 2012-2014) when the August LMW volumes in Barrow Canyon were greater than the 2005-2015 mean (cf. Fig. 3). Conversely, smaller daily sea ice extents and faster/earlier sea ice retreats occurred in years (2005, 2007, 2010, 2011, 2015) when August LMW volumes were less than the 2005-2015 mean. For late ice retreat years, the mean ice edge (20% concentration) on 1 July extended as far south as Point Hope in the eastern Chukchi Sea (Fig. 6a) while for early ice retreat years the mean 1 July ice edge was much further to the north with a distinctive, largely ice-free tongue in the eastern Chukchi, corresponding to the northward path of the warm ACW and CSW (Fig. 6b).

It follows from the yearly ice retreat histories depicted in Figure 5 and the covariant relationships illustrated in Table 1, Figure 3 and Figure 4 that volumes of LMW and WW tend to be proportionately greater and ACW and CSW volumes proportionately less in late ice retreat years. Conversely, volumes of LMW and WW tend to be proportionately less and ACW and CSW volumes proportionately greater in early ice retreat years.

3.2 Wind forcing and sea ice retreat

Yearly differences in the late-summer areal extent of Arctic sea ice have been attributed to differences in wind-induced Ekman drift as mediated by average summer sea level pressure anomalies (e.g. Rogers, 1978; Maslanik et al., 1999; Ogi et al., 2008). Stated another way, summer ice extent represents the net response to wind forcing integrated over a time period of ice retreat. In this section, we explore aspects of the relationships among seasonally-averaged (27 May – 11 August) atmospheric variables (SLP and winds) and sea ice retreat across the eastern Chukchi shelf. We begin with sea ice areas in the eastern Chukchi at the end of the ice retreat season (11 August) for years 2005-2015. East Chukchi ice areas on this date in 2006, 2008, 2010, and 2012-2014 were greater than the 2005-2015 mean ice area and are identified as late retreat years. Ice areas in 2005, 2007, 2009, 2011, and 2015 were less than the 2005-2015 mean and are identified as early retreat years. Note that, based on ice areas at the end of the melt season, 2009 and 2010 are respectively classified as early and late retreat years, whereas 2009 and 2010 are respectively classified as late and early retreat years based on LMW volumes.

The mean seasonally-averaged (27 May - 11 August) SLP field for late ice retreat years (Fig. 7a) shows that the Beaufort Sea High (BSH) is centered adjacent to the Canadian archipelago and that isobars over the Arctic are generally widely-spaced indicating regionally weak mean winds. The companion plot (Fig. 7b) of vector-mean winds (arrows) shows this to be the case while the blue and green shading indicates that the ensemble of daily winds (N = 6 yrs x 77 days/yr = 462 days) exhibits little directional constancy. Directional constancy is defined as the ratio of the N-day vector-mean wind speed to the N-day scalar mean wind speed (Moore, 2003). The mean seasonally-averaged SLP field for early ice retreat years (Fig. 7c), shows a stronger BSH (> 1017 hPa) that is displaced westward and a slightly deeper Siberian Low relative to the late-retreat SLP conditions. The more closely-spaced isobars over the southern Beaufort Sea, northern Chukchi Sea and East Siberian Sea drive stronger (longer arrows), more persistent easterlies (yellow and orange shading) across this region of the Arctic (Figure 7d). End-of-season east Chukchi ice area is therefore positively-correlated with seasonally-averaged U and V winds at statistically-significant levels over most of the study area north of ~70°N (blue and black contours; Figures 7b,d).

3.3 Wind forcing and the Pacific-Arctic pressure head

Seasonally-averaged winds in the southern Chukchi (~66°-69°N) are weak (small arrows), variable (blue and green shading) and not significantly-correlated with ice area (Fig. 7b,d). Because Bering Strait transport is typically modeled as the sum of pressure head-driven and local (in the vicinity of Bering Strait) wind-driven components, these observations suggest that seasonally-averaged local winds are not primarily responsible for year-to-year differences in average transport through the strait during the sea ice retreat season. It follows that the pressure head component might therefore be mediated by remote winds during the ice retreat season. Because the Pacific-Arctic pressure head is attributed to a steric or sea surface height difference between the Bering Sea and Arctic Ocean (Coachman and Aagaard, 1966; Stigebrandt, 1984), we invoke a height proxy derived from wind stress curl for these analyses.

At each oceanic NCEP grid point (i,j) in the study domain and for each survey year t, we use the seasonally-averaged negative Ekman pumping velocity, W_{Ek}, as a proxy for mean steric or sea surface height, h.

$$W_{Ek} = \frac{1}{\rho}\ \vec{k}\ \cdot \nabla \times (\tau / f) \qquad (1)$$

$$h(i,j,t) \approx \alpha\, \overline{-W_{Ek}}\,(i,j,t) \qquad (2)$$

In these two expressions, ρ is a representative sea water density taken to be 1027 kg m^{-3}, τ is the local wind stress, f is the local Coriolis parameter, α is an undetermined constant scale factor and the overbar in expression (2) indicates time-averaging from 27 May to 11 August for year t. At seasonal time scales, Eq. 2 above follows from the time integral of equation 2 in Lagerloef (1995). Because we do not include ice concentration-related effects in our stress calculations and are unable to directly scale sea surface height to the Ekman pumping velocity, only relative changes in sea level and the pressure head can be ascertained from changes in the wind stress curl field. The unknown scale factor α can be eliminated by normalizing the heights

$$H(i,j,t) = \frac{h(i,j,t) - \langle h \rangle}{\max(h) - \min(h)} = \frac{\overline{-W_{Ek}}\ (i,j,t) - \langle \overline{-W_{Ek}} \rangle}{\max\ (\overline{-W_{Ek}}) - \min(\overline{-W_{Ek}})} \qquad (3)$$

in which the brackets, < >, indicate the 11-year mean value. Statistically-significant correlations between WSC-forced sea surface heights and late-summer (11 August) sea ice area in the eastern Chukchi define three centers of action across the western Arctic (Fig. 8). WSC-forced heights in the East Siberian Sea and eastern Beaufort Sea are positively correlated (solid contours) with east

Chukchi sea ice areas, whereas WSC-forced heights in the northern Chukchi Sea are negatively correlated (dashed contour) with east Chukchi sea ice area. In late ice retreat years when wind forcing associated with the BSH is weak (cf. Fig. 7a,b), group-averaged sea surface heights are relatively small everywhere except in the central Beaufort Sea and Gulf of Alaska (Fig. 8a). The relative sea surface slope between the northern Bering shelf and East Siberian Sea is near zero, is positive between the northern Bering shelf and west-central Beaufort Sea and is positive between the northern Bering shelf and eastern Beaufort Sea. In other words, the Pacific-Arctic pressure head is anomalously weak. In early ice retreat years, strong wind forcing (cf. Fig. 7c,d) acts to lower sea level markedly in the East Siberian Sea and raise sea level in the west-central Beaufort Sea (Fig. 8b). Sea level is lowered slightly in the eastern Beaufort Sea. The resulting relative sea surface slopes are negative between the northern Bering shelf and East Siberian Sea, positive between the northern Bering shelf and west-central Beaufort Sea and near zero between the northern Bering shelf and eastern Beaufort Sea. Although not shown, but as might be expected vis a vis Table 1 and Figure 4, broadly similar statistical associations occur for correlations between sea level and the focal water mass volumes as well. We infer from these relationships that yearly differences in wind forcing over the East Siberian Sea/western Chukchi Sea region, mediated by the longitudinal location and strength of the BSH, exert significant control over year-to-year differences in the Pacific-Arctic pressure head.

4. Summary and Discussion

We have shown that late-summer volumes of Pacific-origin and melt water masses in Barrow Canyon are well-correlated with the timing and pattern of sea ice retreat across the Chukchi Sea shelf. These ice retreat characteristics were, in turn, also shown to be well-correlated with the strength of the Pacific-Arctic pressure head as mediated by the strength and longitudinal location of the Beaufort Sea High pressure cell and its associated wind field. These interdependent relationships are summarized in a hierarchical (left to right: driver, response) and comparative (more, less) format in Table 2.

Table 2 *Generalized interdependencies and associations among meteorological, sea ice and oceanographic variables in the Pacific Arctic.*

Sea level pressure	East Siberian/ north Chukchi winds	Sea level and Pacific-Arctic pressure head	Northward heat transport	East Chukchi Sea Ice	Barrow Canyon water masses
Stronger BSH in western Beaufort	Strong, persistent easterlies; stronger WSC	Lower SL in East Siberian Sea; stronger PH	Greater net heat transport along Alaskan Chukchi coast	Early ice retreat; more open water in August	More ACW, CSW; Less LMW, WW
Weaker BSH in eastern Beaufort	Weak, variable easterlies; weaker WSC	Relatively higher SL in East Siberian Sea; weaker PH	Less net heat transport along Alaskan Chukchi coast	Late ice retreat; less open water in August	More LMW, WW; Less ACW, CSW

Relationships among variables listed in Table 2 were directly identified through correlation analyses except for relative differences in northward heat transport which were inferred from year-to-year differences in the timing and pattern of sea ice retreat and differences in ACW volumes. Moreover, we also infer that the difference between transport along this coastal pathway and transport carried through Herald Canyon and the Central Channel during the ice retreat season is greater in early ice retreat years than late retreat years. Underpinning this latter inference is a simple analytical model proposed by Toulany and Garrett (1984) in which slowly-fluctuating flow through a narrow strait connecting two basins is geostrophically-limited by the sea level difference between the basins. A consequence of their model formulation is that, in the adjustment to reduce the sea level difference between basins, the higher sea level signal (in the Bering Sea in the present context) propagates downstream to the lower elevation basin (the

Chukchi Sea) along the coast as a Kelvin wave. Because the amplitude of a Kelvin wave decays exponentially from the coast, the associated geostrophic current is strongest near the Alaskan Chukchi coast. Consequently, a more negative sea surface slope (stronger pressure head) between the Bering and Chukchi Seas drives greater northward volume and property fluxes *along* the Alaskan Chukchi coast (i.e. stronger Alaskan Coastal Current) and promotes the observed earlier ice retreat across the eastern Chukchi shelf (cf. Fig. 6b). The corollary is that a less negative sea surface slope (weaker pressure head) results in weaker volume and property fluxes along the Alaskan Chukchi coast and slower, less directionally-biased ice retreat across the Chukchi shelf (cf. Fig. 6a).

Sea ice cover is also important to the makeup of WW. As mentioned above, our WW mass represented the combination of Remnant Winter Water (RWW; $-1.6°C \leq T < -1°C$, $S \geq 31.5$) and Newly-ventilated Winter Water (NWW; $T < -1.6°C$, $S \geq 31.5$) in the Gong-Pickart classification scheme. In partitioning our combined WW mass into these constituent water masses, we found that NWW and RWW were both present in Barrow Canyon in 2006, 2008, 2009, and 2012-2014; all late ice retreat years (cf. Fig. 6a). However, in 2005, 2007, 2010, 2011, and 2015 (early ice retreat years; Fig. 6b), only RWW was present in Barrow Canyon. Because the transformation of NWW to RWW occurs through mixing with warmer summer waters and/or solar heating (Gong and Pickart, 2015), the presence (absence) of NWW in Barrow in late summer would be a manifestation of late (early) sea ice retreat.

The eleven annual snapshots of Barrow Canyon water mass volumes were the starting point for our correlation analyses. While the water mass volumes embodied in any individual snapshot survey might also be biased by a variety of factors (e.g. local wind-driven circulation, shelf waves, frontal instabilities, internal waves), these potential biasing effects do not fundamentally alter the relationships summarized in Table 2 because any such biasing effects are not entirely random nor are they unconstrained. As mentioned in Section 2.2, our surveys were conducted during locally-weak wind (non-upwelling) conditions. Consequently, random local wind-driven circulation biases were mitigated (cf. Fig. S1) and PH/AW, when present, was largely limited to depths below 120 m (cf. Fig. 2) effectively excluding this water mass from consideration. Perhaps more importantly, particularly as related to the associations summarized in Table 2, our surveys took place at a time during the open-water season when there were occurrences of zero (or very near zero) volumes of LMW (2005, 2007, 2011, 2015; early ice retreat years) and ACW (2006, 2008, 2013, 2014; late ice retreat years). It is unlikely that long waves, instabilities or other factors produced these observed zero/near-zero volumes of LMW and ACW or are able to produce zero/near-zero volumes of WW or CSW. Because our survey line defines a fixed volume across Barrow Canyon, the sum of any noise contributions to a year's volumetric snapshot is zero. Despite uncertainties in our estimations of water mass volumes, the constraints imposed by zero LWM and ACW volumes and resultant associations summarized in Table 2 allow us to reasonably interpret each year's snapshot of water mass volumes as the net (dependent) response to a common period (27 May – 11 August) of integrated or average wind-forcing.

The principal uncertainties in our study results reside in our wind stress calculations and the sea surface height fields derived from them. As noted above, we did not adjust the stress computations to account for ice concentrations directly or through an ice concentration-weighted drag coefficient or to account for internal ice stresses. While height estimates in the East Siberian Sea are significantly-correlated with sea ice area (and Barrow water mass volumes), height estimates in the Bering Sea are not (cf. Fig. 8). Because the normalized sea surface heights over the Bering Sea are very near zero, the Pacific-Arctic pressure head is largely defined by the sea surface heights in the East Siberian Sea and not those in the Bering Sea. Despite these uncertainties, our results are consistent with and complement those of Peralta-Ferriz and Woodgate (2017) who, in a clever use of ocean mass measurements acquired by the Gravity Recovery and Climate Experiment (GRACE) satellite, showed that sea surface height variations in the East Siberian Sea effectively control the magnitude of the Pacific-Arctic pressure head.

From a broader perspective, the observed annual variations in the volumes of the different water masses transiting Barrow Canyon will impact the transfer of properties such as heat, salt, nutrients, and plankton between the Canyon and the northern Chukchi/western Beaufort shelves and the Beaufort Sea that in turn can impact downstream conditions. Low nutrient concentrations are found in the ACW and upper water column across the Canyon during summer, with higher concentrations found at depth in the WW and CSW (e.g., Cota et al., 1996; Codispoti et al., 2013; Danielson et al., 2017). Upwelling in the Canyon can bring nutrients into the upper water column, supporting elevated primary production (e.g., Lowry et al., 2015). Distinct or “indicator” phytoplankton and zooplankton species or types are found in each water mass type (e.g., Hopcroft et al., 2010; Ashjian et al., 2017; Danielson et al., 2017; Pinchuk and Eisner, 2017; Sigler et al., 2017). Much of the zooplankton in the Chukchi Sea is now believed to originate in the Bering Sea (e.g., Wassmann et al., 20125; Ershova et al., 2017; Pinchuk and Eisner, 2017), including the euphausiids that are important prey for bowhead whales (e.g., Ashjian et al., 2010; Moore et al., 2010; Citta et al., 2015). Increased transport of these expatriate species, if they can recruit in Arctic conditions, could change the species composition, and thus ecosystem structure, of the slope and basin (although see Matsuno et al., 2015). The Arctic Marine Pulses (AMP) model explains linkages between the northern Bering and Chukchi shelves and Beaufort shelf break and slope (among other linkages) and postulates that seasonal biophysical pulses coupled to organism phenology are central to explaining ecosystem dynamics (Moore et al., in press). The interannual variability in transport, water mass volumes, and intrinsic physical, chemical, and biological properties through Barrow Canyon observed here embodies that pulse.

Acknowledgments

Many people and organizations contributed to the success of this work. Many thanks to Eugene Brower and the Barrow Whaling Captains Association, the Alaska Eskimo Whaling Commission, North Slope Borough Mayors George Ahmaogak and Edward Itta, and the North Slope Borough Department of Wildlife Management including Taqulik Hepa, Harry Brower Jr., Robert Suydam, Billy Adams, Cyd Hanns, Leslie Pierce, and especially Craig George. The work would not have been possible without the experience and assistance of Bill Kopplin, the captain of the *R/V Annika Marie* and *R/V Ukpik*, and crew members Ned Manning, Mike Johnson, Randy Pollock, Tony D'Aoust, Mike Fleming, Lars Isaac, and Johnny Bjorgaard. Logistics at Utqiagvik and Prudhoe Bay were provided by Glenn Sheehan, Lewis Brower, the Barrow Arctic Science Consortium, UIC Science, Polar Field Services, and British Petroleum. Thanks to our colleagues and collaborators with whom we worked in Utqiagvik including Janet Clarke, Megan

Ferguson, Dave Rugh, Kim Shelden, Mark Baumgartner, Barry Sherr, and Ev Sherr. Teachers Kirk Beckendorf, Jeff Manker, and Lisa Seff participated in the fieldwork through the PolarTREC program at the Arctic Research Consortium of the United States. Graduate students Aaron Hartz and Heather McEachen and Postdoctoral Investigators Leo Bérline and Joel Llopiz also assisted with the fieldwork. We are grateful to Frank Bahr (Woods Hole Oceanographic Institution) for processing the ADCP data. This research was supported by the National Science Foundation through grants PLR-1023331 and OPP-0436131 to C. J. Ashjian, PLR-1022139 and OPP-0436110 to R. G. Campbell, and PLR-1023446 and OPP-043166 to S. R. Okkonen and with funds from the National Oceanic and Atmospheric Administration (NOAA) under cooperative agreement NA08OAR4320751 with the University of Alaska and cooperative agreements NA17RJ1223 and NA09OAR4320129 with the Woods Hole Oceanographic Institution. Support was also provided by the Minerals Management Service (MMS), now Bureau of Ocean Energy Management (BOEM), through Interagency Agreement 0106RU39923 / M08PG20021 between the National Marine Fisheries Service and MMS/BOEM and through the National Oceanographic Partnership Program with award number N00014-08-1-0311 from the Office of Naval Research to the Woods Hole Oceanographic Institution.   Additional support was provided by the Coastal Marine Institute at the University of Alaska and the James M. and Ruth P. Clark Arctic Research Initiative Fund at the Woods Hole Oceanographic Institution. This is contribution #691 from the Scholarly Union of Bio-Physical Arctic Researchers.

References

Ahlnas, K., and G. R. Garrison. 1984. Satellite and oceanographic observations of the warm coastal current in the Chukchi Sea, Arctic, 37, 244–254.

Ashjian, C.J., Braund, S.R., Campbell, R.G., George, J.C., Kruse, J. Maslowski, W., Moore, S.E., Nicolson, C.R., Okkonen, S.R., Sherr, B.F., Sherr, E.B., Spitz, Y. 2010. Climate variability, oceanography, bowhead whale distribution, and Iñupiat subsistence whaling near Barrow, AK. Arctic 63: 179-194.

Ashjian, C.J., Campbell, R.G., Gelfman, C., Alatalo, P., Elliott, S.M. 2017. Mesozooplankton abundance and distribution in association with hydrography on Hanna Shoal, NE Chukchi Sea, during August 2012 and 2013. Deep-Sea Research II, 144: 21-36, https://doi.org/10.1016/j.dsr2.2017.08.012

Asplin, M.G., J.V. Lukovich, and D.G. Barber. 2009. Atmospheric forcing of the Beaufort Sea ice gyre: Surface pressure climatology and sea ice motion. J. Geophys. Res. 114,C00A06,doi.10.1029/2008JC005127

Brugler, E.T., Pickart, R.S., Moore, G.W.K., Roberts, S., Weingartner, T.J., Statscewich, H. Seasonal to interannual variability of the Pacific water boundary current in the Beaufort Sea. 2014. Prog. Oceanogr. 127, 1-20. http://dx.doi.org/10.1016/j.pocean.2014.05.002

Citta, J. Quakenbush, L.T., Okkonen, S.R., Druckenmiller, M.L., Maslowski, W., Clement-Kinney, J., Ashjian, C.J., George, J.C., Brower, H., Small, R.J., Harwood, L.A., Heide-Jorgensen, M.P. 2015. Ecological characteristics of core areas used by western Arctic bowhead whales, 2006-2012. Prog. Oceanography DOI: 10.1016/j.pocean.2014.08.012

Coachman, L.K. and K. Aagaard. 1966. On the water exchange through Bering Strait. Limnology Oceanography 11 (1), 44–59.

Coachman, L.K., and Aagaard,K.,1988. Transports through Bering Strait: annual and interannual variability. J. Geophys. Res. 93 (C12), 15535–15539.

Codispoti, L.A., Kelly, V., Thessen, A., Matrai, P., Suttles,S., Hill, V., Steele, M., Light, B. 2013. Synthesis of primary production in the Arctic Ocean: III. Nitrate and phosphate based estimates of net community production. Prog. Oceanogr. 110, 126–150. http://dx.doi.org/10.1016/j.pocean.2012.11.006.

Cota, G.F.,Pomeroy, L.R., Harrison,W.G., Jones, E.P., Peters, F., Sheldon, W.M., Weingartner, T.R.. 1996. Nutrients, primary production and microbial hetero- trophy in the southeastern Chukchi Sea: Arctic summer nutrient depletion and heterotrophy. Mar. Ecol. Prog. Ser.135, 247–258.

Danielson, Sl.L., Eisner, L., Ladd, C., Mordy, C., Sousa, L., Weingartner, T.J., 2017. A comparison between late summer 2012 and 2013 water masses, macronutrients, and phytoplankton standing crops in the northern Bering and Chukchi Seas. Deep-Sea Research II 135, 7-26.

Ershova, E.A., Hopcroft, R.R., Kosobokova, K.M., Matsuno, K., Nelson, R.J., Yamaguchi, A., Eisner, L.B. 2015. Long-term changes in summer zooplankton communities of the western Chukchi Sea, 1945-2012. Oceanography 28, 100-115.

Gong, D., Pickart, R.S., 2015. Summertime circulation in the eastern Chukchi Sea. Deep-Sea Research II 118, 18–31.

Hibler III, W.D., 1980. A dynamic thermodynamic sea ice model. J. Phys. Oceanogr. 10, 815–846.

Itoh, M., Nishino, S., Kawaguchi, Y., Kikuchi, T. 2013. Barrow Canyon volume, heat, and freshwater fluxes revealed by long-term mooring observations between 2000 and 2008. J. Geophys. Res. Oceans 118, 4363–4379. http://dx.doi.org/ 10.1002/jgrc.20290.

Itoh, M., Pickart, R.S., Kikuchi, T., Fukamachi, Y., Ohshima, K.I., Simizu, D., Arrigo, K.R., Vagle, S., He, J., Ashjian, C., Mathis, J.T., Nishino, S., Nobre, C. ,2015. Water properties, heat and volume fluxes of Pacific water in Barrow Canyon during summer 2010. J. Geophys. Res. 102,43–54.

Kalnay, E., Kanamitsu, M., Kistler, R., Collins, W., Deaven, D., Gandin, L., Iredell, M., Saha, S., White, G., Woollen, J., Zhu, Y., Leetmaa, A., Reynolds, R., Chelliah, M., Ebisuzaki, W., Higgins, W., Janowiak, J., Mo, K.C., Ropelewski, C., Wang, J., Jenne, R., Joseph, D., 1996. The NCEP/NCAR 40-year reanalysis project. Bulletin of the American Meteorological Society 77, 437–470.

Lagerloef, G.S.E., 1995. Interdecadal variations in the Alaska gyre. J. Phys. Oceanogr. 25, 2242–2258.

Lowry, K.E., Pickart, R.S., Mills, M.M., Brown, Z.W., van Dijken, G.L., Bates, N.R., Arrigo, K.R. 2015. The influence of winter water on phytoplankton blooms in the Chukchi Sea. Deep-Sea research II 118: 53-72. https://doi.org/10.1016/j.dsr2.2015.06.006

Martin, S., Drucker, R., 1997. The effect of possible Taylor columns on the summer ice retreat in the Chukchi Sea. Journal of Geophysical Research 102, 10473–10482.

Martin, T., M. Steele, and J. Zhang. 2014. Seasonality and long-term trend of Arctic Ocean surface stress in a model, J. Geophys. Res. Oceans, 119, 1723–1738, doi:10.1002/ 2013JC009425.

Maslanik, J.A., Serreze, M.C., Agnew, T., 1999. On the record reduction in 1998 Western Arctic Sea-ice cover. Geophysical Research Letters 26 (13), 1905–1908.

Matsuno, K., Yamaguchi, A., Hirawake, T., Nishino, S., Inoue, J., and T. Kikuchi, 2015. Reproductive success of copepods in the Arctic Ocean and the possibility of changes in the Arctic ecosystem. Polar Biology 39: 1075-1079.

Moore, G.W.K., 2003. Gale force winds over the Irminger Sea to the East of Cape Farewell Greenland. Geophys. Res. Lett. 30, 184–187.

Moore, S.E., George, J.C., Sheffield, G., Bacon, J., and C.J. Ashjian, 2010. Bowhead whale distribution and feeding in the western Alaskan Beaufort Sea during late summer, 2005-2006. Arctic 63, 195-205.

Moore, S.E., P.J. Stabeno, J.M. Grebmeier, S.R. Okkonen. 2016. The Arctic Marine Pulses Model: linking annual oceanographic processes to contiguous ecological domains in the Pacific Arctic. Deep-Sea Res. II, http://dx.doi.org/10.1016/j.dsr2.2016.10.011 (in press)

Mountain, D. G., L. K. Coachman, and K. Aagaard, 1976. On the flow through Barrow Canyon, J. Phys. Oceanogr., 6, 461– 470.

Okkonen, S.R., C. Ashjian, R.G. Campbell, W. Maslowski, J.L. Clement-Kinney, and R. Potter. 2009. Intrusion of warm Bering/Chukchi waters onto the western Beaufort Shelf, J. Geophys. Res, 114,C00A11,doi.10.1029/2008JC004870

Paquette, R.G. and Bourke, R.H., 1974. Observations on the coastal current of arctic Alaska. Journal of Marine Research 32, 195–207.

Peralta-Ferriz, C. and R.A. Woodgate. 2017. The dominant role of the East Siberian Sea in driving the oceanic flow through the Bering Strait – conclusions from GRACE ocean mass satellite data and *in situ* mooring observations between 2002 and 2016. Geophys. Res. Lett. doi: 10.1002/2017GL075179

Perovich, D., B. Light, H. Eicken, K. Jones, K. Runciman, and S. Nghiem (2007), Increasing solar heating of the Arctic Ocean and adjacent seas, 1979–2005: Attribution and role in the ice-albedo feedback, Geophys. Res. Lett., 34, L19505, doi:10.1029/2007GL031480.

Pickart, R.S., G.W.K. Moore, C. Mao, F. Bahr, C. Nobre, T.J. Weingartner. 2016. Circulation of winter water on the Chukchi shelf in early Summer. Deep-Sea Res. II. 130:56–75.

Pinchuk, A.I., Eisner, L.B. 2017. Spatial heterogeneity in zooplankton summer distribution in the eastern Chukchi Sea in 2012-2013 as a result of large-scale interactions of water masses. Deep-Sea Research II, in press. http:/dx.doi.org/10.1016/j/dsr2/2016/11/003.

Reynolds, R. W., Smith, T.M., Liu, C., Chelton, D.B., Casey, K.S., Schlax, M.G. 2007: Daily High-Resolution-Blended Analyses for Sea Surface Temperature. J. Climate, 20, 5473-5496.

Sigler, M.F., Mueter, F.J., Bluhm, B.A., Busy, M.S., Cokelet, E.D., Danielson, S.L.,de Robertis, A. Eisner, L.B., Farley E.V., Iken, K., Kuletz, K.J., Lauth, R.R., Logerwell, E.A., Pinchuk, E.I.

2017. Late summer zoogeography of the northern Bering and Chukchi seas. Deep-Sea Research II 135, 168-189.

Spall, M.A., 2007. Circulation and water mass transformation in a model of the Chukchi Sea. J. Geophys. Res. 112, C05025.

Springer, A.M., McRoy, C.P. 1993. The paradox of pelagic food webs in the northern Bering Sea III. Patterns of primary production. Cont. Shelf Res., 13(5-6):575-599.

Stigebrandt, A., 1984. The North Pacific: a global-scale estuary. J. Phys. Oceanogr. 14, 464–470.

Toulany, B., Garrett, C. 1984. Geostrophic control of fluctuating barotropic flow through straits. J. Phys. Oceanogr. 14, 649-655.

Walsh, J.J., McRoy, C.P., Coachman, L.K., Goering, J.J., Nihoul, J.J., Whitledge, T.E., Blackburn, T.H., Springer, A.M., Tripp, R.D., Hansell, D.A., Djenidi, S., Deleersnijder, H.K., Lund, B.A., Andersen, P., Muller-Karger, F.E., Dean, K.K., (1989) Carbon and nitrogen cycling within the Bering/Chukchi Seas: source regions for organic matter effecting AOU demands of the Arctic Ocean. Progr. in Oceanogr. 22, 277–359.

Wassman, Pl, Kosobokova, K. N., Slagstad, D., Drinkwater, D.F., Hopcroft, R.R., Moore, S.E., Ellingsen, I., Nelson, R.J., Carmack, E, Popova, E., Berge, J. 2015. The contiguous domains of Arctic Ocean advection: Trails of life and death. Prog. Oceanogr. 139: 42-65.

Weingartner, T.J., Aagaard, K., Woodgate, R.A., Danielson, S., Sasaki, Y., Cavalieri, D., 2005. Circulation on the north central Chukchi Sea shelf. Deep-Sea Res. II, (doi:10.1016/j.dsr2.2005.10.015).

Weingartner, T.J., Dobbins, E., Danielson, S., Winsor, P., Potter, R., Statscewich, H., 2013. Hydrographic variability over the northeastern Chukchi Sea shelf in summer-fall 2008-2010. Cont. Shelf Res., 67: 5-22.

Winsor, P., Chapman, D.C., 2004. Pathways of Pacific water across the Chukchi Sea: a numerical model study. J. Geophys. Res. 109 (C3), C03002, (doi:10.1029/2003JC001962).

Woodgate, R.A., Aagaard, K., Weingartner, T., 2005. A year in the physical oceanography of the Chukchi Sea: moored measurements from autumn 1990–91. Deep-Sea Res. II, (doi:10.1016/j.dsr2.2005.10.016).

Figure Captions

Figure 1 A) *Map of the Pacific-Arctic region with place names. The dashed line delineates the 10°-wide box within which daily sea ice areas were calculated. The solid line delineates the Barrow Canyon area within the Pacific-Arctic region. B) The location of the hydrographic survey line across Barrow Canyon (black line) in relation to the DBO 5 line (grey line).*

Figure 2 *Annual water mass sections across Barrow Canyon. Sections are viewed looking northeastward, down-canyon. Point Barrow lies at the right hand side of the plots. LMW=Late season Melt Water, EMW=Early season Melt Water, ACW=Alaskan Coastal Water, CSW=Chukchi Summer Water, WW=Winter Water, PH/AW=Polar Halocline/Atlantic Water.*

Figure 3 *Panels A-D) Annual volume anomalies relative to the 2005-2015 mean volumes for each of the four focal water masses. Panel E) Annual east Chukchi sea ice areas on 1 July (black) and on 11 August (grey). The horizontal lines indicate the 2005-2015 mean ice areas for these dates.*

Figure 4 *Correlations among Barrow Canyon water mass volumes and daily sea ice areas on the Chukchi shelf between 169°W-159°W. Grey shading between 27 May and 11 August defines a representative sea ice retreat season. Horizontal lines at +/- 0.521 and +/- 0.685 indicate statistically-significant correlations at $p<0.05$ and $p<0.01$, respectively (9 degrees of freedom). The vertical lines in August identify the dates of annual hydrographic surveys in Barrow Canyon.*

Figure 5 *Annual records of daily sea ice areas on the Chukchi shelf between 169°W-159°W. Solid lines and boldface years indicate ice area histories for years in which LMW anomalies are positive. Dotted lines indicate ice area histories for years in which LMW anomalies are negative. Blue shading between 27 May and 11 August defines a representative sea ice retreat season. The vertical lines in August identify the dates of annual hydrographic surveys in Barrow Canyon.*

Figure 6 *Mean Chukchi Sea ice edges (20% ice concentrations) on 1 July and 1 August for late ice retreat years (A) and early ice retreat years (B). Late retreat years are associated with LMW volumes greater than the 2005-2015 mean. Early retreat years are associated with LMW volumes less than the 2005-2015 mean. Dotted line contours delineate the 150-m and 1000-m isobaths. The dashed line delineates the 10°-wide box within which daily sea ice areas were calculated.*

Figure 7 *Mean seasonal (27-May-11 August) atmospheric circulation for late ice retreat years (A, B) and early ice retreat years (C,D). A) and C) display mean sea level pressure (SLP) patterns. The blue crosses indicate the NCEP grid points at which the mean pressure associated with the Beaufort Sea High (BSH) is maximum. B and D display mean wind vectors, directional constancy (colored shading), and statistically-significant correlations between ice areas and U-component winds (blue contours) and V-component winds (black contours). Correlation contours at $r = 0.521$ ($p<0.05$), 0.685 ($p<0.01$), and 0.735 ($p<0.005$).*

Figure 8 *Normalized mean WSC-forced sea surface heights (color shading) for (A) late ice retreat years and (B) early ice retreat years. The solid grey line delineates the zero-height contour. Black contours identify statistically-significant correlations ($r = +/- 0.521, 0.685, 0.735$; $p<0.05, 0.01, 0.005$) between sea surface heights and late-summer (11 August) east Chukchi Sea ice areas. Solid black contours indicate positive correlations. Dashed black lines indicate negative correlations.*

Figure S1 *Annual along-canyon (65°T – 245°T) velocity sections acquired by a towed 300 kHz acoustic Doppler current profiler. Contour interval is 25 cm s^{-1}. Solid contours and shaded areas indicate down-canyon (to 65°T) velocities. Dotted contours indicate up-canyon (to 245°T) velocities. Sections are viewed looking northeastward, down-canyon. Point Barrow lies at the right hand side of the plots. No velocity data were acquired during the 2009 survey due to a failure of the ADCP.*

Figure S2 *Annual temperature sections across Barrow Canyon. Contour interval is 1°C. Sections are viewed looking northeastward, down-canyon. Point Barrow lies at the right hand side of the plots.*

Figure S3 *Annual salinity sections across Barrow Canyon. Contour interval is 1 psu. Sections are viewed looking northeastward, down-canyon. Point Barrow lies at the right hand side of the plots.*

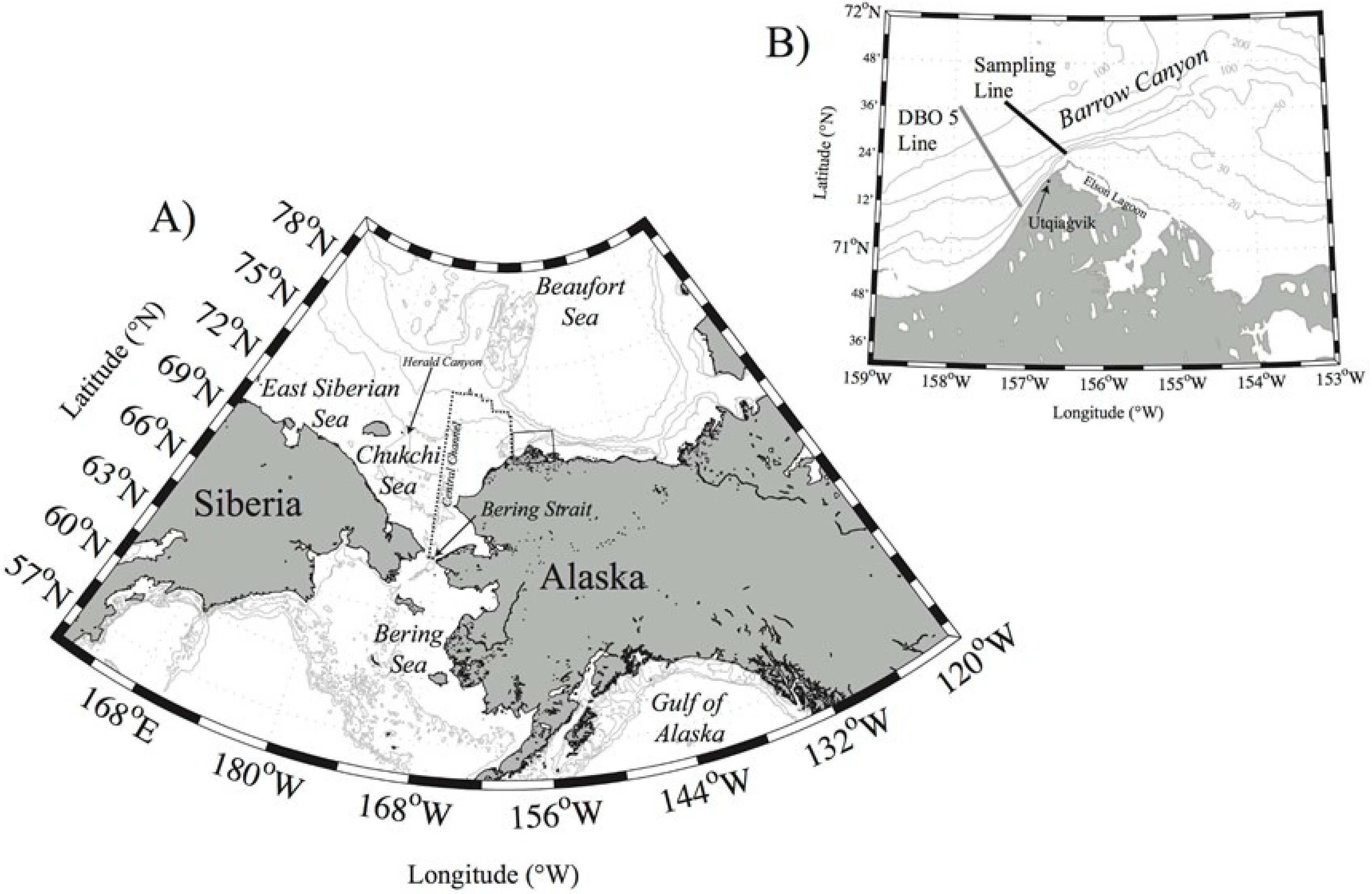
A)
78°N
75°N
72°N
69°N
66°N
63°N
60°N
57°N
Latitude (°N)
Beaufort Sea
Herald Canyon
East Siberian Sea
Chukchi Sea
Central Channel
Bering Strait
Siberia
Alaska
Bering Sea
Gulf of Alaska
168°E
180°W
168°W
156°W
144°W
132°W
120°W
Longitude (°W)
B)
72°N
48'
36'
24'
12'
71°N
48'
36'
Latitude (°N)
Sampling Line
Barrow Canyon
DBO 5 Line
Elson Lagoon
Utqiaġvik
100
200
100
50
30
20
159°W
158°W
157°W
156°W
155°W
154°W
153°W
Longitude (°W)

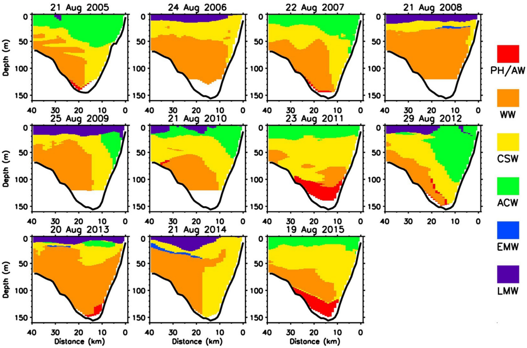
21 Aug 2005
24 Aug 2006
22 Aug 2007
21 Aug 2008
25 Aug 2009
21 Aug 2010
23 Aug 2011
29 Aug 2012
20 Aug 2013
21 Aug 2014
19 Aug 2015
Depth (m)
0
50
100
150
Distance (km)
40
30
20
10
0
PH/AW
WW
CSW
ACW
EMW
LMW

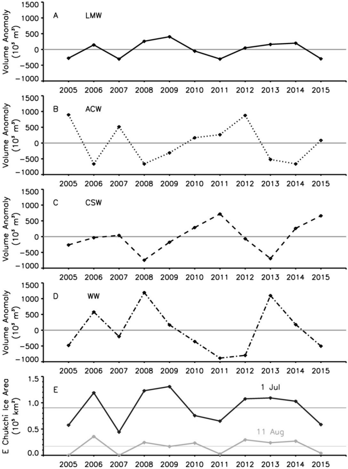
A
LMW
B
ACW
C
CSW
D
WW
E
Volume Anomaly $(10^5\ m^3)$
1500
1000
500
0
−500
−1000
2005
2006
2007
2008
2009
2010
2011
2012
2013
2014
2015
E Chukchi Ice Area $(10^5\ km^2)$
1.5
1.0
0.5
0.0
1 Jul
11 Aug

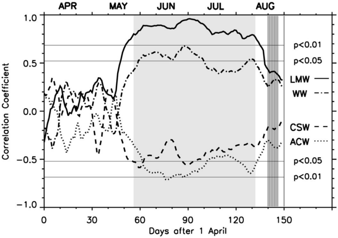
APR
MAY
JUN
JUL
AUG
Correlation Coefficient
1.0
0.5
0.0
−0.5
−1.0
0
30
60
90
120
150
Days after 1 April
p<0.01
p<0.05
LMW
WW
CSW
ACW
p<0.05
p<0.01

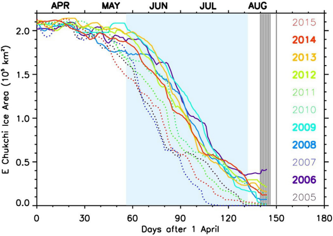
APR
MAY
JUN
JUL
AUG
2015
2014
2013
2012
2011
2010
2009
2008
2007
2006
2005
E Chukchi Ice Area (10^3 km²)
2.0
1.5
1.0
0.5
0.0
0
30
60
90
120
150
180
Days after 1 April

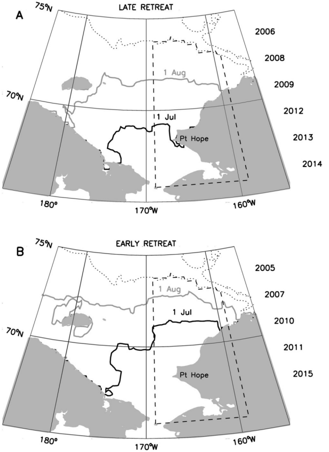
A
LATE RETREAT
75°N
70°N
65°N
180°
170°W
160°W
1 Aug
1 Jul
Pt Hope
2006
2008
2009
2012
2013
2014
B
EARLY RETREAT
75°N
70°N
65°N
180°
170°W
160°W
1 Aug
1 Jul
Pt Hope
2005
2007
2010
2011
2015

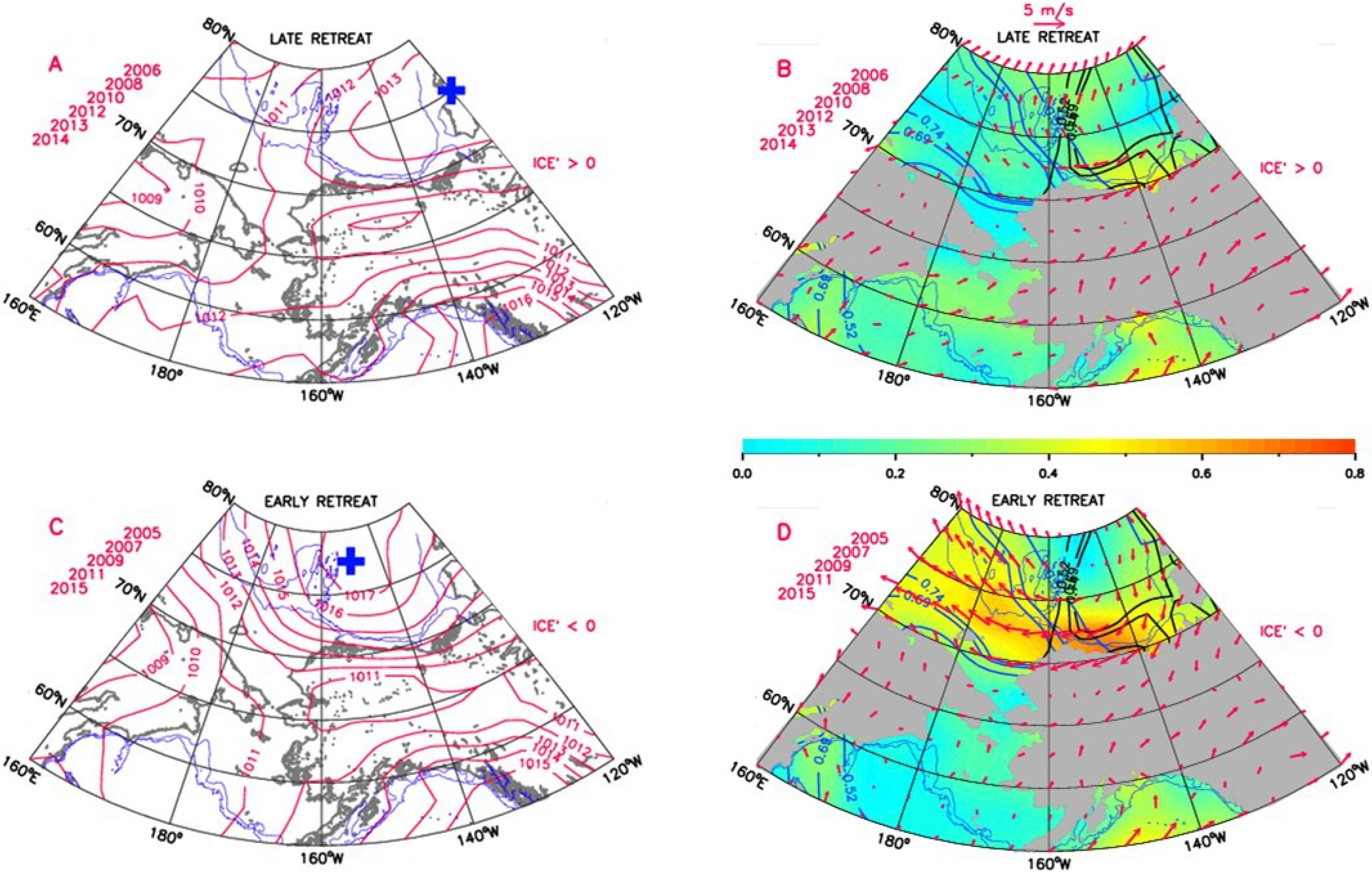
A
LATE RETREAT
2006
2008
2010
2012
2013
2014
ICE' > 0
80°N
70°N
60°N
160°E
180°
160°W
140°W
120°W
1009
1010
1011
1012
1013
1014
1015
1016
B
5 m/s
LATE RETREAT
2006
2008
2010
2012
2013
2014
ICE' > 0
0.74
0.69
0.52
0.0
0.2
0.4
0.6
0.8
C
EARLY RETREAT
2005
2007
2009
2011
2015
ICE' < 0
1009
1010
1011
1012
1013
1014
1015
1016
1017
D
EARLY RETREAT
2005
2007
2009
2011
2015
ICE' < 0
0.74
0.69
0.52

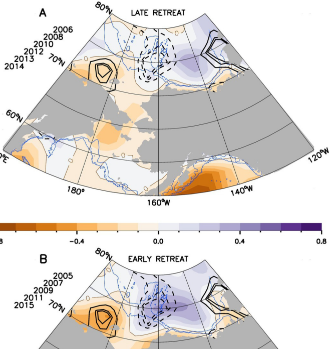
A
80°N
LATE RETREAT
2006
2008
2010
2012
2013
2014
70°N
60°N
160°E
180°
160°W
140°W
120°W
−0.8
−0.4
0.0
0.4
0.8
B
80°N
EARLY RETREAT
2005
2007
2009
2011
2015
70°N
60°N
160°E
180°
160°W
140°W
120°W